

Sources and effects of electrode impedance during deep brain stimulation

Christopher R. Butson, Christopher B. Maks, Cameron C. McIntyre *

Department of Biomedical Engineering, Cleveland Clinic Foundation, 9500 Euclid Ave. ND-20, Cleveland, OH 44195, USA

Accepted 8 October 2005

Available online 22 December 2005

Abstract

Objective: Clinical impedance measurements for deep brain stimulation (DBS) electrodes in human patients are normally in the range 500–1500 Ω . DBS devices utilize voltage-controlled stimulation; therefore, the current delivered to the tissue is inversely proportional to the impedance. The goals of this study were to evaluate the effects of various electrical properties of the tissue medium and electrode-tissue interface on the impedance and to determine the impact of clinically relevant impedance variability on the volume of tissue activated (VTA) during DBS.

Methods: Axisymmetric finite-element models (FEM) of the DBS system were constructed with explicit representation of encapsulation layers around the electrode and implanted pulse generator. Impedance was calculated by dividing the stimulation voltage by the integrated current density along the active electrode contact. The models utilized a Fourier FEM solver that accounted for the capacitive components of the electrode-tissue interface during voltage-controlled stimulation. The resulting time- and space-dependent voltage waveforms generated in the tissue medium were superimposed onto cable model axons to calculate the VTA.

Results: The primary determinants of electrode impedance were the thickness and conductivity of the encapsulation layer around the electrode contact and the conductivity of the bulk tissue medium. The difference in the VTA between our low (790 Ω) and high (1244 Ω) impedance models with typical DBS settings (–3 V, 90 μ s, 130 Hz pulse train) was 121 mm³, representing a 52% volume reduction.

Conclusions: Electrode impedance has a substantial effect on the VTA and accurate representation of electrode impedance should be an explicit component of computational models of voltage-controlled DBS.

Significance: Impedance is often used to identify broken leads (for values >2000 Ω) or short circuits in the hardware (for values <50 Ω); however, clinical impedance values also represent an important parameter in defining the spread of stimulation during DBS.

© 2005 International Federation of Clinical Neurophysiology. Published by Elsevier Ireland Ltd. All rights reserved.

Keywords: Electrode-tissue interface; Tissue encapsulation; Voltage-controlled stimulation; Deep brain stimulation

1. Introduction

Deep brain stimulation (DBS) represents an established therapy for essential tremor (Benabid et al., 1996), Parkinson's disease (Obeso et al., 2001), and dystonia (Vidailhet et al., 2005). In addition, DBS shows promise in the treatment of epilepsy (Hodaie et al., 2002), obsessive-compulsive disorder (Gabriels et al., 2003), and depression (Mayberg et al., 2005). However, the clinical successes of DBS are tempered by our limited understanding of the effects of DBS on the nervous system.

Converging theoretical (McIntyre et al., 2004a) and experimental (Hashimoto et al., 2003) results suggest that DBS generates an excitatory effect on axons surrounding the electrode. While correlations between axonal activation and the therapeutic mechanisms of DBS remain controversial, one leading hypothesis is that high frequency stimulation results in an override of the underlying pathological neural activity patterns (Grill et al., 2004; Hashimoto et al., 2003; McIntyre et al., 2004b; Montgomery and Baker, 2000). However, a wide range of factors can influence the clinical response to DBS including the disease state of the patient, anatomical target selected for stimulation, location of the electrode within the target, electrode geometry, and selection of the stimulation parameters (voltage, pulse

* Corresponding author. Tel.: +1 216 445 3264; fax: +1 216 444 9198.
E-mail address: mcintyc@ccf.org (C.C. McIntyre).

width, and frequency). In addition, existing clinical DBS devices utilize voltage-controlled stimulation and as a result the amount of current delivered to the tissue is dependent on the electrode impedance. Clinical measurements of DBS electrode impedance typically range from 500–1500 Ω (Obeso et al., 2001; Volkmann et al., 2002); however it is presently unclear what factors influence this variability and how this range of electrode impedance affects the spatial extent of neural stimulation.

Several factors contribute to impedance values, including: the connections between the implanted pulse generator (IPG) and electrode; the surface area of the electrode(s) and IPG; the conductivity and thickness of the encapsulation layers that surround the electrode(s) and IPG; and the conductivity of the bulk tissue medium. The quadripolar Medtronic 3387/3389 electrode and IPG systems are currently the only FDA approved clinical DBS devices. The Itrel II and Soletra IPGs can record impedances of up to 2,000 Ω , while the Kinetra measures up to 4,000 Ω . High impedance values are often associated with lead breakage or some other mechanical failure, especially if the current is less than 15 μ A. Alternately, very low impedance values (< 50 Ω) with high current levels (> 250 mA) are associated with short circuits in the hardware. In between these extremes, little clinical attention is typically paid to the impedance when selecting therapeutic stimulation parameter settings for individual patients. However, the large range of impedances suggests that current delivery and the subsequent neural response to DBS could be substantially different from patient-to-patient and from contact-to-contact.

In previous work we have provided quantitative predictions of the volume of tissue activated (VTA) during DBS (Butson and McIntyre, 2005; McIntyre et al., 2004a,c); however, these studies ignored the impact of impedance variability. In this study we explored the sensitivity of electrode impedance to changes in the properties of electrode(s) and tissue medium. Our fundamental goals were to define a physical basis for the 500–1500 Ω range typically observed with clinical DBS and to determine how this impedance variability affects the VTA.

2. Methods

This study addressed the origin and impact of electrode impedance in DBS with a primary focus on the electrode-tissue interface. A range of detailed computer models were developed with various geometrical and electrical properties to characterize likely sources of impedance variability in clinical DBS devices. Models of neurostimulation that integrate finite-element based electric field solutions and multi-compartment cable models of myelinated axons were used to predict the VTA generated by DBS under different impedance conditions.

2.1. Deep brain stimulation finite element model

Axisymmetric finite element models (FEM) with \sim 80,000 nodes were created with FEMLAB 3.1 (COMSOL Inc., Burlington, MA) to represent the DBS electrode and surrounding tissue medium (Fig. 1). The DBS electrode lead and a single electrode contact were centered on the z-axis, surrounded by the tissue medium. The indifferent electrode was placed on the outer boundary of the axisymmetric model and designed to match the surface area of the IPG (\sim 56.5 cm²). Several models were created to explore the effects of different geometrical properties and conductivities on DBS impedance. All models contained a cathode (the DBS electrode contact) and anode (the indifferent or return electrode of the IPG case) to mimic the monopolar stimulation condition commonly used in clinical practice. Variable density FEM meshes were used to maximize solution accuracy; mesh density was highest where the electric field gradient was largest. The voltage within the volume was determined using a Fourier FEM solver which solves the Poisson equation in time and space simultaneously (Butson and McIntyre, 2005). The purpose of this solver was to combine the actual DBS waveform and the capacitance of the electrode-tissue interface into the bioelectric field model. Briefly, the Poisson equation was solved using direct matrix inversion (UMFPACK solver) at 512 frequencies between 0 Hz (DC) and 5000 Hz to determine the potential distribution (V_e) generated within the tissue medium (stiffness matrix σ) based on a collection of sources (I):

$$\nabla \cdot \sigma \nabla V_e = -I$$

The Fourier FEM solver used the solution of the Poisson equation at each component frequency along with the fast Fourier transform (FFT) of the stimulation waveform to determine the time dependent waveform at each point in the axisymmetric volume.

2.2. Impedance model

We explored the sensitivity of electrode impedance to several model parameters by manipulating a standard model specified in Table 1 and Fig. 1. The standard model had an impedance of 1003 Ω . The model was used to analyze the sensitivity of impedance to changes in dimensions of the volume conductor. Variations in length (L) from 50–300 mm and height (H) from 20–120 mm were intended to reflect the path of allowable current flow between the IPG and the electrode contact(s) through the tissue medium. The length could be viewed as the distance from electrode contact to IPG, while the height reflects the diameter of the head and neck. Tissue conductivity (σ_T) was varied from 0.15–0.3 S/m, derived from previous experimental ranges (Geddes and Baker, 1967; Malmivuo and Plonsey, 1995; Ranck, 1963). We

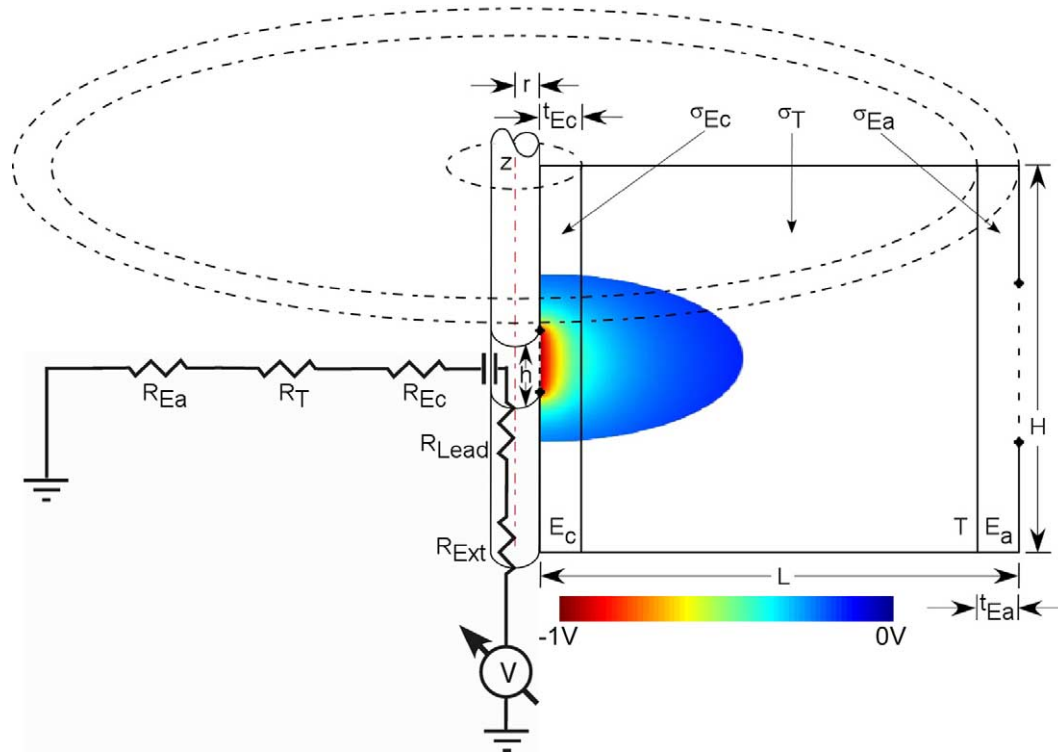


Fig. 1. Axisymmetric model of DBS. The right side shows the DBS electrode (centered on the z -axis) surrounded by a volume conductor that includes an electrode encapsulation layer (Ec), bulk tissue medium (T), and IPG encapsulation layer (Ea). FEM mesh and voltage solution are shown as colored area adjacent to electrode for -1 V stimulus. Model parameters were: volume conductor height (H) and length (L); encapsulation thickness around the electrode lead (t_{Ec}) and IPG (t_{Ea}); electrode contact height (h) and radius (r); bulk tissue conductivity (σ_T), electrode encapsulation conductivity (σ_{Ec}) and IPG encapsulation conductivity (σ_{Ea}). The left side shows an equivalent circuit model of DBS system including -1 V source, extension wire (R_{Ext} , 40Ω), lead wire (R_{Lead} , 40Ω), electrode contact capacitance (C), electrode encapsulation layer (R_{Ec}), bulk tissue (R_T) and IPG encapsulation layer (R_{Ea}).

also explored the effects of electrode contact size. The dimensions of the cylindrical Medtronic 3387/3389 DBS electrode contacts are specified as 1.5 mm height by 1.27 mm diameter. However, these values can vary up to 0.1 mm in height or diameter due to manufacturing tolerances (Moss et al., 2004). Finally, we varied the thickness and conductivity of the encapsulation layer around the electrode contact (t_{Ec} and σ_{Ec} respectively) and IPG (t_{Ea} and σ_{Ea} , respectively). Encapsulation thickness ranged from 0–1 mm (Haberler et al., 2000; Moss et al., 2004), and encapsulation conductivity ranged from 0.05–0.2 S/m (Grill and Mortimer, 1994).

For each model, a -1 V DC stimulus was applied between the cathodal contact and the IPG, and the voltage distribution within the volume was determined. Current density was integrated around the contact surface to determine the current injected into the volume. Ohms law was used to determine the impedance from $Z=V/I$. Fig. 1 shows an equivalent circuit diagram of the model DBS system. To enable a more accurate comparison with clinical DBS impedance measurements, an 80Ω wire resistance and the capacitance of the electrode contact were present in the model (Butson and McIntyre, 2005; Holsheimer et al., 2000). All model impedances were calculated at the onset of the cathodic phase of the stimulation pulse. In turn, these

values were independent of voltage or pulse width. This is in contrast to the known dependence of impedance on stimulation parameters for both the Medtronic telemetry device and the DBS electrode (see Section 4).

2.3. Estimation of the volume of tissue activated

Field-axon simulations were conducted using Fourier FEM DBS electrode models coupled to $5.7 \mu\text{m}$ diameter

Table 1
Impedance model

| Parameter | Standard value | Range |
|--|----------------|----------------|
| Volume conductor height (H) | 40 mm | 20–120 mm |
| Volume conductor length (L) | 120 mm | 50–300 mm |
| Electrode encapsulation thickness (t_{Ec}) | 0.5 mm | 0.1–1.0 mm |
| IPG Encapsulation thickness (t_{Ea}) | 0.5 mm | 0.0–1.0 mm |
| Electrode contact height (h) | 1.5 mm | 1.4–1.6 mm |
| Electrode contact radius (r) | 0.635 mm | 0.585–0.685 mm |
| Contact encapsulation conductivity (σ_{Ec}) | 0.1 S/m | 0.05–0.2 S/m |
| Tissue conductivity (σ_T) | 0.2 S/m | 0.15–0.3 S/m |
| IPG encapsulation conductivity (σ_{Ea}) | 0.1 S/m | 0.05–0.15 S/m |

Impedance model: standard parameter values and range of variation.

myelinated axon models (Butson and McIntyre, 2005; McIntyre et al., 2002). A collection of 119 model axons were distributed in a 17×7 matrix oriented perpendicular to the electrode shaft. This orientation of axons was used to identify the spatial extent of activation in the vertical and horizontal directions relative to the electrode shaft (localization of activation in axons oriented parallel to the shaft would be ambiguous in the vertical direction). The axons were placed from 1 to 4 mm lateral to the electrode and from +4 mm above to -4 mm below the center of the electrode contact. Each model axon included 21 nodes of Ranvier with 0.5 mm internodal spacing.

The stimulus waveforms used in our model were based on the Medtronic Irel II IPG. The waveforms were biphasic and charge-balanced with a cathodic pulse equal to the user defined pulse width followed by an anodic recharge pulse. The anodic pulse began 0.4 ms after the end of the cathodic pulse and ended 4 ms before the beginning of the next cathodic pulse. The IPG output voltage was equal to the peak-to-peak voltage between cathodic and anodic phases of the stimulus waveform. The time-dependent potential distribution generated in the tissue medium from the Fourier FEM solution was interpolated onto the length of each cable model, and the time-dependent transmembrane potential variations induced by the stimulation were calculated in NEURON v5.7 (Hines and Carnevale, 1997). Threshold stimulus amplitudes were defined that generated action potentials in a one-to-one ratio with the stimulus frequency. The threshold stimulus values were used to create 2D contours to define the boundary of activation as a function of the stimulus amplitude. These contours were swept around the axis of the electrode to determine the VTA volume. 3D renderings and VTA calculations relative to the thalamus were performed using BioPSE (Scientific Computing and Imaging Institute, University of Utah).

3. Results

The fundamental goals of this study were to identify factors that influence DBS electrode impedance and to quantify the effects of impedance variability on the VTA during voltage-controlled DBS.

3.1. Effects of the volume conductor geometry on impedance

Variations in dimensions of the overall volume conductor model had a weak effect on impedance values. Increases in model length (L) over the range 50–300 mm caused an increase of $\Delta Z \approx 38 \Omega$; increases in height (H) from 20–120 mm caused a decrease of $\Delta Z \approx 48 \Omega$ (Fig. 2(A)). While these parameters have nonzero effects on impedance, they are unlikely to account for the range observed in clinical measurements.

3.2. Effects of electrode dimensions on impedance

Changes in the surface area of the electrode contact, resulting from manufacturing tolerances, caused the impedance to vary by $\Delta Z \approx 85 \Omega$, with impedance values equally sensitive to changes in either contact height or diameter. Results are shown for impedance as a function of surface area as height and diameter are varied ± 0.1 mm from their standard values (Fig. 2(B)). By combining the smallest and largest combinations of height and diameter we calculated impedance values of 1094Ω for $d = 1.17$ mm, $h = 1.4$ mm and 922Ω for $d = 1.37$ mm, $h = 1.6$ mm ($\Delta Z \approx 172 \Omega$). Hence, manufacturing variability in electrode dimensions could be a contributor to clinical impedance variability.

3.3. Effects of conductivity on impedance

Conductivity values were varied over the range 0.15–0.3 S/m for the bulk tissue medium (σ_T), 0.05–0.15 S/m for the encapsulation around the IPG (σ_{Ea}) and 0.05–0.2 S/m around the electrode contact (σ_{Ec}). Over our examined ranges, increasing conductivity in the bulk tissue medium decreased impedance by $\Delta Z \approx 250 \Omega$ and increasing conductivity of the electrode lead encapsulation decreased impedance by $\Delta Z \approx 800 \Omega$ (Fig. 2(C)). In contrast, encapsulation around the IPG had almost no effect with a change of $\Delta Z < 1 \Omega$. The nearly linear relationships between resistivity and impedance for each of these variables are shown in the inset of Fig. 2(C). Hence, σ_T and σ_{Ec} have a strong effect on impedance; however, the data needed to accurately estimate the variance of these values from patient to patient, or within one patient over time are not presently available.

3.4. Effects of encapsulation thickness on impedance

Encapsulation thickness around the IPG had almost no effect on impedance with a change of $\Delta Z < 1 \Omega$ over a range 0 to 1 mm. In contrast, encapsulation thickness around the electrode shaft had a strong effect on impedance. Variations in t_{Ec} caused changes of $\Delta Z \approx 450 \Omega$ (Fig. 2(D)). Hence, encapsulation around the electrode lead but not the IPG had a strong effect on impedance.

3.5. Clinically relevant impedance models

The various model parameters were compiled according to the magnitude of their effects. Using this data we constructed three models to represent the range of impedance values observed clinically. These three models were used in subsequent simulations to evaluate the effects of impedance changes on the VTA. The models are specified as follows: low impedance model, 741Ω , $\sigma_{Ec} = 0.2$ S/m, $t_{Ec} = 0.5$ mm; medium impedance model, 1003Ω ,

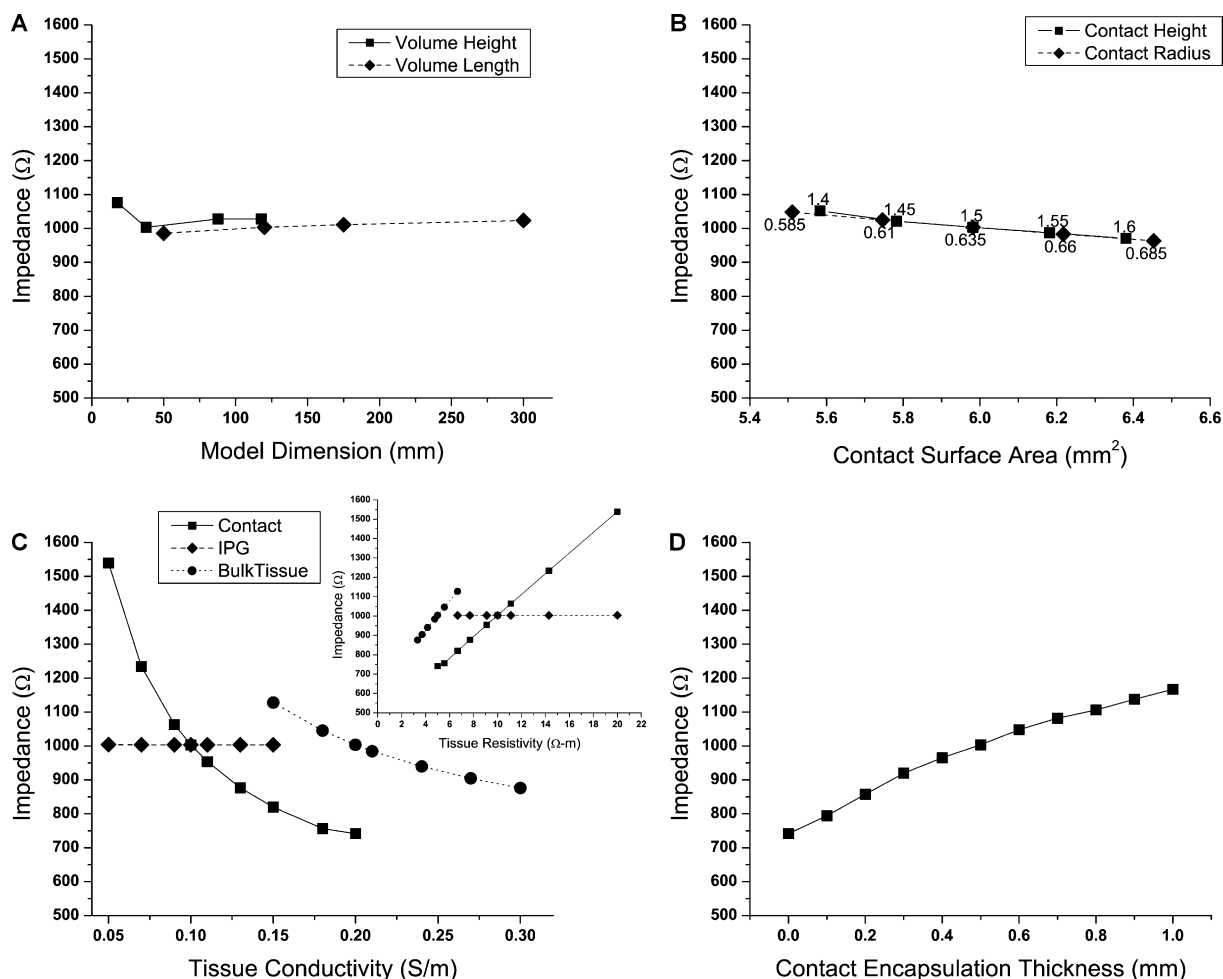


Fig. 2. Impedance sensitivity. (A) Impedance as a function of the volume conductor dimensions (height and length). (B) Impedance as a function of the electrode contact surface area resulting from changes in both height and diameter. (C) Impedance as a function of conductivity for the bulk tissue medium, electrode encapsulation, and IPG encapsulation relative to the standard model geometry. Inset shows impedance versus resistivity for the same data. (D) Impedance as a function of the encapsulation thickness on the IPG or electrode. In each plot, all model parameters were defined in Table 1, and only the listed parameter was changed.

$\sigma_{Ec} = 0.1 \text{ S/m}$, $t_{Ec} = 0.5 \text{ mm}$; high impedance model, $1244 \text{ } \Omega$, $\sigma_{Ec} = 0.07 \text{ S/m}$, $t_{Ec} = 0.5 \text{ mm}$.

3.6. Impedance modulates shape and extent of the VTA

The low, medium, and high impedance models generated substantially different VTAs with clinically relevant stimulation parameter settings (-1.5 to -3 V pulse amplitude, $90 \text{ } \mu\text{s}$ pulse duration, 130 Hz stimulus train) (Fig. 3(A)). We found that the spread of activation was inversely correlated with the impedance value. VTA volumes were 230 , 146 , and 110 mm^3 for the low, medium and high impedance models at -3 V stimulation, respectively. The reduction in VTA volume with increasing impedance was related to the reduction in both the vertical and lateral spread of the stimulus (Fig. 3(A)). Current densities at the electrode contact, and the corresponding charge densities, were also inversely correlated with impedance values. The average charge densities for

-3 V , $90 \text{ } \mu\text{s}$ stimulus pulses in the low, medium and high impedance models were 6 , 4.5 and $3.6 \text{ } \mu\text{C}/\text{cm}^2/\text{phase}$, respectively. These values are well below the $30 \text{ } \mu\text{C}/\text{cm}^2/\text{phase}$ limit for safe stimulation but would increase linearly with increases in voltage or pulse width. For comparison purposes, Fig. 3(B) displays 3D renderings of the VTAs for the low and high impedance stimulation models at -3 V in the context of thalamic DBS.

4. Discussion

Electrode impedance plays an important role in defining the current delivered to the tissue during voltage-controlled DBS. Within the assumptions of our model (see below), the results of this study suggest that much of the impedance variability commonly recorded with clinical DBS devices can be accounted for with varying degrees of tissue encapsulation. Impedance values were most sensitive to

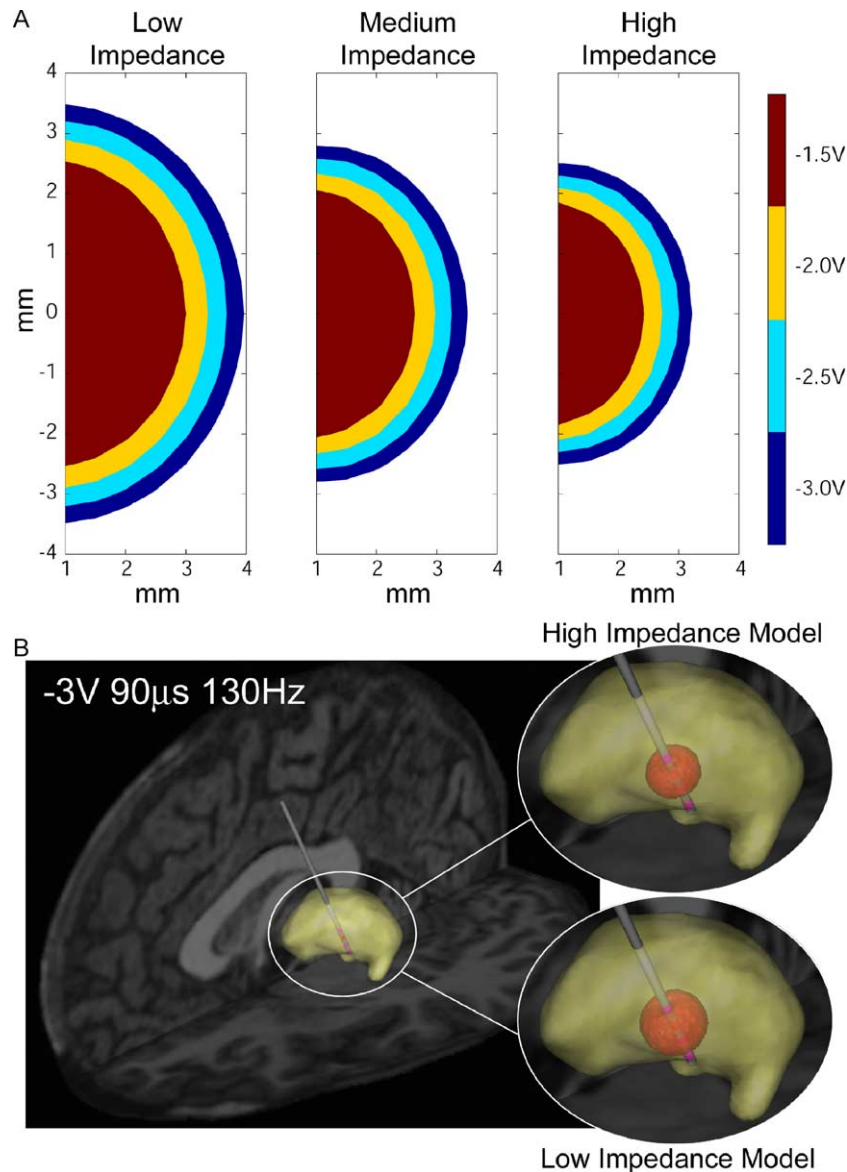


Fig. 3. Volume of tissue activated. (A) spatial plot of axisymmetric stimulation spread for common DBS stimulus settings (-1.5 , -2 , -2.5 or -3 V pulse amplitude; 130 Hz; $90 \mu\text{s}$ pulse width) using the low, medium and high impedance models. (B) 3D model of Medtronic 3387 DBS electrode implanted in thalamus shown relative to sagittal and axial MRI slices. VTAs are shown for the high (top right) and low (bottom right) impedance models.

the thickness and conductivity of the encapsulation around the electrode contact. Lower encapsulation conductivities and thicker encapsulation layers reduce the VTA by increasing the voltage gradient within the encapsulation, thereby decreasing the stimulating influence of the applied electric field within the bulk tissue medium. Our results show that clinically relevant impedance variability can substantially alter the VTA size and shape for typical therapeutic stimulation parameter settings. Therefore, future attempts to quantify the spread of stimulation in DBS should explicitly incorporate electrode impedance in the calculations and consideration should be given to the electrode impedance when selecting therapeutic stimulation parameter settings for individual patients.

This study only considered sources of impedance variability resulting from the volume conductor and the size of the electrode. Other sources could also have substantial effects on impedance. For example, the $\sim 80 \Omega$ impedance of the Medtronic lead and extension wiring (Hemm et al., 2004; Holsheimer et al., 2000) can increase dramatically due to poor mechanical or electrical coupling between the IPG and the extension, or between the extension and lead. Additionally, each of the four individual wires within the extension and lead are made up of a group of individual filars, and breakage of one or more of these filars can dramatically increase resistance. Increases in impedance resulting from these hardware issues will reduce the voltage drop within the tissue medium, which will reduce the VTA.

Monopolar and bipolar stimulation result in different impedance values. Our model predicts that impedance values during bipolar stimulation will always be higher than monopolar stimulation. In the standard model, with the cathode and anode on adjacent electrode contacts, the Medtronic 3389 (0.5 mm contact spacing) and 3387 electrodes (1.5 mm contact spacing) had model impedances of 1478 and 1641 Ω , respectively. Adding an inactive contact between the cathode and anode increased the impedance to $>2000 \Omega$ for either electrode type. Similar to the monopolar stimulation results, bipolar impedances were most strongly influenced by the encapsulation layer around the electrode contact, and by the tissue conductivity.

Our model is designed to simulate a chronic and stable DBS electrode-tissue interface. The use of homogeneous isotropic subdomains of the encapsulation and bulk tissue medium are gross simplifications of the three-dimensionally complex tissue micro- and macro-structure surrounding implanted electrodes (Haberler et al., 2000; McIntyre et al., 2004c; Moss et al., 2004). In turn, a more accurate representation of the tissue medium will undoubtedly introduce additional variability in the impedance. Further, we assume the electrode surface is perfectly smooth and ignore any electrode corrosion and surface modification that may occur as a result of prolonged stimulation (Merrill et al., 2005). Hence, the surface area specified in our electrode models represents an underestimate of the actual surface area of clinical electrodes. However, analysis of post-mortem or explanted DBS electrodes does not show any visible surface modification of the metal electrode contacts (Haberler et al., 2000; Hemm et al., 2004; Moss et al., 2004).

The results of this study suggest that tissue conductivity plays an important role in DBS impedance measurements; however, a great deal of variability exists within the currently available estimates. Mean values have been put forth as 0.15 S/m for white matter, 0.45 S/m for gray matter and 0.17 S/m as a mean conductivity (Geddes and Baker, 1967; Malmivuo and Plonsey, 1995). Another common value for mean conductivity is 0.3 S/m (Ranck, 1963). However, variation in human brain conductivity has only been examined in a single study. Back and Alesch (Back and Alesch, 2003) used the four electrode technique ((Grill and Mortimer, 1994) similar to a field plethysmograph) with *in vivo* DBS to show that tissue impedances can vary up to 33.3% from patient-to-patient.

An additional source of variability is the conductivity of the electrode encapsulation. Encapsulation is the final stage of the foreign body reaction, wherein the body attempts to destroy or isolate any non-native substance. The tissue response includes both an early anti-inflammatory response due to insertion trauma and a sustained response induced in part by the interplay among micromotion, tethering, and device biocompatibility (Johnson et al., 2005). Prior studies have indicated that encapsulation thickness around the DBS electrode lead is at least 25 μm and no greater

than 1 mm (Haberler et al., 2000; Hemm et al., 2004). Haberler et al. (Haberler et al., 2000) performed post-mortem histological examination of the brains of eight patients who were stimulated up to 70 months. They used a variety of stains and antibodies to examine myelin sheaths, connective tissue, axons, fibrillary astrogliosis, glial fibrillary acidic protein, neurofilament protein, synaptophysin and microglia. They found similar results in all patients who underwent long-term stimulation. Tissue changes around the active contact and nonstimulated areas adjacent to the insulated parts of the lead did not differ. Around the lead track, a thin inner capsule of connective tissue was noted. The thickness of this fibrous sheath ranged from 5 to 25 μm , with no correlation to duration of stimulation. A narrow rim of fibrillary gliosis of less than 500 μm abutted the fibrous capsule. In the adjacent brain tissue, a zone of less than 1 mm showed loosely scattered glial fibrillary acidic protein-positive protein astrocytes. They concluded that clinical long-lasting benefit of DBS correlates with the absence of progressive gliotic scar formation. Nevertheless, gliosis and/or the giant cell reaction is likely to alter tissue impedance and distort current distribution (Moss et al., 2004) (Figs. 2 and 3).

Also of interest is a phenomenon where stimulation appears to transiently decrease electrode impedance. Hemm et al. (Hemm et al., 2004) reported a statistically significant difference of $\sim 430 \Omega$ between active and inactive DBS contacts during chronic stimulation. Further, they observed a reversible drop in impedance when contacts were activated with monopolar stimulation over a period of several days. Upon deactivating the contact, the impedance would return to the pre-stimulation values. This effect only occurred *in vivo*, as they were unable to duplicate these results with an electrode in a saline bath. These results could be explained by work from Johnson et al. (Johnson et al., 2005) who found that the most substantial and consistent impedance change came from protein adsorption and the cellular layers surrounding the electrode. In turn, stimulation through a given contact can modify the tissue microstructure of the local encapsulation, increasing conductivity and decreasing electrode impedance.

The impedance values reported in this paper were calculated using Ohm's law. Specifically, the voltage at the onset of the cathodic stimulation pulse was divided by the current, where current was calculated by integrating the current density across the electrode contact. The values calculated with this method are consistent with those reported using the Medtronic DBS programmer with either the Itrel II or Soletra IPGs. By default, these devices measure impedance at -1.5 V , 210 μs , 30 Hz. In experiments where the IPG case and a DBS electrode were connected with a 1 k Ω resistor, the Medtronic programmer accurately reported the resistance value with these stimulation parameters. However, it is noteworthy that measured impedance was a function of both the voltage and

pulse width generated by the Medtronic IPG. Increases in either parameter caused a decrease in the measured impedance. This is in contrast to the results of Holsheimer et al. (Holsheimer et al., 2000) who reported increased impedance values with longer pulse widths for DBS electrodes in a saline bath driven by a function generator. This disparity is most likely due to differences in the way impedances are measured from the time-dependent voltage waveform.

In summary, the clinical impedance measurements from DBS electrodes are dependent on a long list of factors, many of which cannot be directly measured. However, our theoretical analysis suggests that much of the 500–1500 Ω range seen clinically can be accounted for with simple but realistic variability in the electrical properties of the electrode encapsulation and bulk tissue medium. Impedance changes within this clinical range can directly affect the size and shape of the VTA. In turn, attempts to quantify the stimulation effects of DBS on a patient-by-patient basis should explicitly account for the measured electrode impedance.

Acknowledgements

This work was supported by grants from the American Parkinson Disease Association, the Ohio Biomedical Research and Technology Transfer Partnership, and the National Institutes of Health (NS-50449 & NS-52042). The authors would like to thank Scott Kokones for helpful discussion on this project and Jaimie Henderson for providing the 3D thalamic reconstruction.

References

- Back C, Alesch F. Postoperative monitoring of the electrical properties of tissue and electrodes in deep brain stimulation. *Neuromodulation* 2003; 6:248–53.
- Benabid AL, Pollak P, Gao D, Hoffmann D, Limousin P, Gay E, Payen I, Benazzouz A. Chronic electrical stimulation of the ventralis inter-medius nucleus of the thalamus as a treatment of movement disorders. *J Neurosurg* 1996;84:203–14.
- Butson CR, McIntyre CC. Tissue and electrode capacitance reduce neural activation volumes during deep brain stimulation. *Clin Neurophysiol* 2005;116:2490–500.
- Gabriels L, Cosyns P, Nuttin B, Demeulemeester H, Gybels J. Deep brain stimulation for treatment-refractory obsessive-compulsive disorder: psychopathological and neuropsychological outcome in three cases. *Acta Psychiatr Scand* 2003;107:275–82.
- Geddes LA, Baker LE. The specific resistance of biological material—a compendium of data for the biomedical engineer and physiologist. *Med Biol Eng* 1967;5:271–93.
- Grill WM, Mortimer JT. Electrical properties of implant encapsulation tissue. *Ann Biomed Eng* 1994;22:23–33.
- Grill WM, Snyder AN, Miocinovic S. Deep brain stimulation creates an informational lesion of the stimulated nucleus. *NeuroReport* 2004;15: 1137–40.
- Haberler C, Alesch F, Mazal PR, Pilz P, Jellinger K, Pinter MM, Hainfellner JA, Budka H. No tissue damage by chronic deep brain stimulation in Parkinson's disease. *Ann Neurol* 2000;48:372–6.
- Hashimoto T, Elder CM, Okun MS, Patrick SK, Vitek JL. Stimulation of the subthalamic nucleus changes the firing pattern of pallidal neurons. *J Neurosci* 2003;23:1916–23.
- Hemm S, Vayssiere N, Mennessier G, Cif L, Zanca M, Ravel P, Frerebeau P, Coubes P. Evolution of brain impedance in dystonic patients treated by GPi electrical stimulation. *Neuromodulation* 2004;7: 67–75.
- Hines ML, Carnevale NT. The NEURON simulation environment. *Neural Comput* 1997;9:1179–209.
- Hodaie M, Wennberg RA, Dostrovsky JO, Lozano AM. Chronic anterior thalamus stimulation for intractable epilepsy. *Epilepsia* 2002;43:603–8.
- Holsheimer J, Dijkstra EA, Demeulemeester H, Nuttin B. Chronaxie calculated from current-duration and voltage-duration data. *J Neurosci Methods* 2000;97:45–50.
- Johnson MD, Otto KJ, Kipke DR. Repeated voltage biasing improves unit recordings by reducing resistive tissue impedances. *IEEE Trans Neural Syst Rehabil Eng* 2005;13:160–5.
- Malmivuo J, Plonsey R. *Bioelectromagnetism: principles and applications of bioelectric and biomagnetic fields*. New York: Oxford University Press; 1995.
- Mayberg HS, Lozano AM, Voon V, McNeely HE, Seminowicz D, Hamani C, Schwab JM, Kennedy SH. Deep brain stimulation for treatment-resistant depression. *Neuron* 2005;45:651–60.
- McIntyre CC, Richardson AG, Grill WM. Modeling the excitability of mammalian nerve fibers: influence of afterpotentials on the recovery cycle. *J Neurophysiol* 2002;87:995–1006.
- McIntyre CC, Grill WM, Sherman DL, Thakor NV. Cellular effects of deep brain stimulation: model-based analysis of activation and inhibition. *J Neurophysiol* 2004a;91:1457–69.
- McIntyre CC, Savasta M, Walter BL, Vitek JL. How does deep brain stimulation work? Present understanding and future questions. *J Clin Neurophysiol* 2004b;21:40–50.
- McIntyre CC, Mori S, Sherman DL, Thakor NV, Vitek JL. Electric field and stimulating influence generated by deep brain stimulation of the subthalamic nucleus. *Clin Neurophysiol* 2004c;115:589–95.
- Merrill DR, Bikson M, Jefferys JG. Electrical stimulation of excitable tissue: design of efficacious and safe protocols. *J Neurosci Methods* 2005;141:171–98.
- Montgomery Jr EB, Baker KB. Mechanisms of deep brain stimulation and future technical developments. *Neurol Res* 2000;22:259–66.
- Moss J, Ryder T, Aziz TZ, Graeber MB, Bain PG. Electron microscopy of tissue adherent to explanted electrodes in dystonia and Parkinson's disease. *Brain* 2004;127:2755–63.
- Obeso JA, Olanow CW, Rodriguez-Oroz MC, Krack P, Kumar R, Lang AE. Deep-brain stimulation of the subthalamic nucleus or the pars interna of the globus pallidus in Parkinson's disease. *N Engl J Med* 2001;345: 956–63.
- Ranck Jr JB. Specific impedance of rabbit cerebral cortex. *Exp Neurol* 1963;7:144–52.
- Vidalhet M, Verceuil L, Houeto JL, Krystkowiak P, Benabid AL, Cornu P, Lagrange C, Tezenas du Montcel S, Dormont D, Grand S, Blond S, Detante O, Pillon B, Ardouin C, Agid Y, Destee A, Pollak P. Bilateral deep-brain stimulation of the globus pallidus in primary generalized dystonia. *N Engl J Med* 2005;352:459–67.
- Volkman J, Herzog J, Kopper F, Deuschl G. Introduction to the programming of deep brain stimulators. *Mov Disord* 2002;17:S181–7.